Experimental and computational study of the ultraviolet photolysis of vinylacetylene. Part II.†‡

Jaime A. Stearns,§[a] Timothy S. Zwier,*[a] Elfriede Kraka[c] and Dieter Cremer*[cb]

The ultraviolet photochemistry of vinylacetylene (C_4H_4) was studied under temperature and pressure conditions similar to Titan's atmosphere by exciting the molecule in a constrained expansion that opens into the ion source region of a time-of-flight mass spectrometer. The primary dissociation products detected by vacuum-ultraviolet ionization were found to be C_4H_3 and C_4H_2, in a ratio of 3–10 : 1. Subsequent reaction of the C_4H_3 radicals with the parent C_4H_4 produced two major secondary products: C_8H_6 and C_6H_4. The former was spectroscopically identified as phenylacetylene, confirming that photochemical reactions of C_4H_4 can produce aromatic molecules. The primary dissociation reaction was also studied computationally. The results were consistent with the experimental findings for C_4H_2 and C_4H_3. However, the major product is C_2H_2, which is undetected by 118 nm photoionization in the present experiment but should account for roughly two-thirds of the products. Simulations were also performed to confirm that the present experiment accurately represents the 220 nm photochemistry of vinylacetylene at the temperature and pressure of Titan's atmosphere, with a product yield of $C_2H_2 : C_4H_2 : C_4H_3$ of 66 : 7 : 27. Accounting for the wavelength dependent solar flux on Titan, the estimated absorption cross section of vinylacetylene in the ultraviolet, and the slightly wavelength dependent product distribution, the overall product yield predicted by the simulations for ultraviolet photolysis of vinylacetylene on Titan is $C_2H_2 : C_4H_2 : C_4H_3 = 65 : 8 : 27$. Finally, a simulation was performed under conditions of a shock tube experiment to examine the differences between thermal and photochemical dissociation. The product yield of this simulation was $C_2H_2 : C_4H_2 : C_4H_3 = 61 : 1 : 38$.

I. Introduction

In flames and planetary atmospheres, small unsaturated hydrocarbons play key roles as seeds for the formation of aromatic and polycyclic aromatic hydrocarbons. Saturn's moon Titan is well known for its dense haze, which is thought to be composed of large hydrocarbon and nitrile molecules, formed by photochemistry of smaller species.[1–4] The recent detection of benzene on Titan has led to increased interest in the mechanisms of aromatic formation in Titan's atmosphere.[4–6] The arrival of the Cassini mission to Saturn in 2004 and the release of the Huygens probe in early 2005 have already provided new data on the atmosphere of Titan, including mass spectrometric results indicating a wealth of species up to mass 140.[7–9] As these larger hydrocarbons are

identified, the photochemistry of smaller molecules will continue to be studied to account for their formation.

C_4 hydrocarbons such as diacetylene and butadiene are among the largest photochemically active molecules considered in models of Titan's atmosphere. Both are likely candidates for involvement in the formation of aromatics. Our laboratory has previously studied the reactions of metastable diacetylene with itself and other hydrocarbons for incorporation into models of Titan.[10–13] Of particular interest was the reaction between metastable diacetylene and 1,3-butadiene, which produced benzene and phenylacetylene. The primary photochemistry of butadiene has also been studied. The major product was found to be propargyl radical,[14] which is thought to be a major source of benzene *via* radical–radical recombination.[4,6] Investigations into the secondary reactions of butadiene photoproducts are currently underway.[15]

In addition to diacetylene and butadiene, vinylacetylene must also be considered in the family of photochemically active C_4 hydrocarbons. Despite (or perhaps because of) its similar size, electronic structure, and reactivity, vinylacetylene has not been studied as thoroughly as the other C_4 systems. In models of Titan's atmosphere, the behavior of C_4H_4 is inferred from analogous reactions of C_4H_2 and C_4H_6, rather than based on experimental data. Two prominent models of Titan's atmosphere included photolysis of vinylacetylene to form acetylene and diacetylene, with the branching ratio for C_4H_2

[a] *Department of Chemistry, Purdue University, West Lafayette, IN 47907. E-mail: zwier@purdue.edu*
[b] *Department of Chemistry and Department of Physics, University of the Pacific, Stockton, CA 95211*
[c] *Department of Chemistry, University of the Pacific, Stockton, CA 95211. E-mail: dcremer@pacific.edu*

being nearly four times greater than that for C_2H_2.[1,4] Other models either include only the diacetylene product[2] or do not include photolysis of vinylacetylene at all.[3] Absorption cross sections of vinylacetylene in the region of 160–260 nm were recently measured as a function of temperature.[16] These results have been incorporated into photochemical models, although the lowest temperatures studied were still well above atmospheric conditions on Titan.[4]

Even under the cold conditions of the supersonic expansion, vinylacetylene has a broad, unstructured absorption beginning around 222 nm and increasing to the blue past the range of our photoexcitation laser system. 1,3-Butadiene has a similar absorption spectrum, the breadth of which is explained by rapid internal conversion to the ground state *via* two conical intersections.[14] Diacetylene, by contrast, has broadened but vibronically-resolved transitions beginning around 250 nm, and the photophysics is dominated by intersystem crossing rather than internal conversion.[17,18] Furthermore, in the case of diacetylene, the lowest bond dissociation energy is above the wavelength range of its major ultraviolet absorption, so even if internal conversion occurs it does not lead to free radical products.[17] Because of the similarities between the spectra of vinylacetylene and 1,3-butadiene, it is likely that they undergo similar photophysical processes. However, further experimental and computational exploration of this point is warranted.

Although the photochemistry of other, less stable, C_4H_4 isomers has been studied in an argon matrix, vinylacetylene was not the primary reactant in these studies.[19,20] The only studies of the unimolecular dissociation of vinylacetylene have been under the high-temperature conditions of shock tube pyrolysis. One comprehensive study identified three dissociation pathways and their initial reaction rate expressions.[21] At a typical temperature of 1500 K, those rates are

$$C_4H_4 \rightarrow C_4H_3 + H \quad 12.8\,\mathrm{s}^{-1}$$
$$\rightarrow 2C_2H_2 \quad 184.3\,\mathrm{s}^{-1} \quad (1)$$
$$\rightarrow C_4H_2 + H_2 \quad 20.0\,\mathrm{s}^{-1}$$
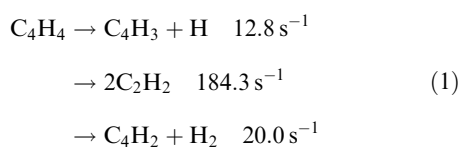
The ratio of C_2H_2 to C_4H_2 was found by end product analysis to be 7–10 : 1, while the rate constants of the three initiating reactions heavily favored production of C_2H_2. These results are in stark contrast to the behavior of C_4H_4 used in models of Titan's atmosphere, where C_4H_2 is assumed to be the major product.[1,2,4] In the shock tube study,[21] the C_2H_2 and C_4H_2 products were followed in time by absorption at 230 nm and by gas chromatography, but the radical reaction channel could only be inferred by simulating the kinetics of the entire system.

One goal of the present work is to detect the primary products of unimolecular decomposition of vinylacetylene directly by mass spectrometry. Photolyzing vinylacetylene inside a small reaction tube outside the nozzle of a supersonic jet pulsed-valve allows any reactions to proceed only as long as the traversal time of the reaction tube, approximately 15 μs, after which the mixture is expanded into the vacuum chamber. The reaction products are identified by vacuum ultraviolet laser ionization time-of-flight mass spectrometry. Acetylene is anticipated to be a major product, based on the shock tube studies.[21] Unfortunately, our experimental detection method

(using 10.5 eV light) does not allow for detection of C_2H_2 due to its high ionization potential (11.4 eV[22]). This deficiency will be addressed by a theoretical study of the dissociation of vinylacetylene under the conditions of our reaction tube. A detailed ground state Potential Energy Surface (PES) for C_4H_4 has been calculated in Paper I.[23] In the simulations presented here, we have assumed that vinylacetylene, like 1,3-butadiene, undergoes rapid internal conversion following ultraviolet excitation, and that dissociation occurs subsequently on the ground state singlet PES. A simulation of the system using this PES will allow us to predict the importance of the acetylene product channel.

Furthermore, this theoretical approach allows us to assess the differences between the conditions of our reaction tube, Titan's atmosphere, and a shock tube pyrolysis experiment. Typical temperatures in the shock tube studies are between 1000–2500 K, while Titan's atmosphere at an altitude of 100 km has a temperature of approximately 150 K.[24] The role of collisional cooling is also very different between the shock tube experiments, which are often carried out near 1 bar, and Titan's atmosphere, which at 100 km has a pressure of approximately 10 mbar.[24] Rate constants derived at high temperature are frequently extrapolated to the much colder temperatures of Titan's atmosphere because of the lack of any other data. A recent study of the mechanisms of benzene formation in Titan's atmosphere demonstrated that the benzene mole fraction was quite sensitive to the rate constants used, but frequently room temperature rate constants were used due to the lack of low temperature results.[6] An understanding of the appropriate rate constants is crucial to the correct modeling of Titan's atmosphere. As will be shown below, the conditions of the reaction tube in the present experiment are very similar to those of Titan's atmosphere. The combination of experiment and theory will also serve the larger goal of understanding the differences between high temperature thermal dissociation and low temperature ultraviolet photodissociation.

Although the dilute gas mixture in the present experiment ensures that primary products dominate, secondary reaction products can also be identified. In particular, we are interested in identifying novel routes to aromatic ring formation from photolysis of small hydrocarbons. The role of even-carbon hydrocarbons in the formation of aromatics in combustion chemistry, and, by extension, planetary atmospheres, has long been debated.[25–27] One specific issue is the importance of the C_4H_5 and C_4H_3 radicals relative to their odd-carbon counterpart propargyl radical (C_3H_3). Here we present spectroscopic evidence that the aromatic molecule phenylacetylene is a product of the photochemistry of vinylacetylene under conditions very similar to those of Titan's atmosphere. We first identify the C_4H_3 radical as a primary dissociation product, then identify C_6H_4 and C_8H_6 as major secondary reaction products. Finally, the C_8H_6 molecule is spectroscopically identified as phenylacetylene.

II. Experimental methods

The supersonic jet time-of-flight mass spectrometry technique used for the photochemistry experiments has been described

previously.[13] Briefly, vinylacetylene was seeded as a 7% mixture in helium at 2.5 bar and expanded through a home-built piezo valve into a 1 cm-long reaction tube of 2 mm diameter. Inside the reaction tube, the molecules were excited by sending a 220 nm laser pulse into the tube, counterpropa-gating the constrained expansion. The source of the 220 nm light was the frequency doubled output of a Radiant Dyes dye laser pumped by the third harmonic of a Nd:YAG laser, giving a photolysis laser power of 0.2 mJ pulse^{-1}. The photoexcita-tion wavelength was chosen to give the best photochemical yield as determined by the trade-off between the absorption spectrum of vinylacetylene and the available laser power.

During the $\sim$15 μs traversal of the reaction tube, any reactive species produced by vinylacetylene dissociation could undergo collisions either with the buffer gas or other radicals or molecules. These secondary reactions were quenched at the end of the reaction tube by the final expansion of the gas mixture into the vacuum chamber. The total number density inside the reaction tube was estimated to be 7×10^{16} molecules cm^{-3} for a typical flow rate of 3.4×10^{-5} L· bar sec^{-1} and a 300 μs gas pulse operating at 20 Hz.

Following a $\sim$70 μs travel time into the ion source region, the products were photoionized and detected by time-of-flight mass spectrometry. Difference mass spectra were obtained by recording the mass spectrum with and without the photoexci-tation laser, and subtracting to give a spectrum of just the photoproducts. Each mass spectrum was an average of 512 or 1000 shots, and several spectra were averaged. Ionization was accomplished by vacuum ultraviolet light provided by the ninth harmonic of the Nd:YAG laser. This light is generated by taking the third harmonic at 355 nm into a 1 m tube filled with 16 torr of xenon and 177 torr of argon (for phase matching), in which the 355 nm light is frequency tripled to 118 nm, equivalent to 10.5 eV photon energy.[11,28] This is a general ionization technique that rarely results in fragmenta-tion, and so is an excellent method for determining the molecular weights of the photoproducts. Action spectroscopy (not shown) was used to determine that the wavelength dependence of the photoproduct signals was in accord with the onset of the vinylacetylene absorption over the range 225–218 nm. Resonant two-photon ionization spectroscopy was used to record ultraviolet spectra of the photoproducts in favorable cases.

The photoproduct signals were a few percent of the size of the parent molecule signal. To enhance detection of photo-products, the parent ions were pulsed away using an ion gate pulser placed 15 cm in front of the detector. The device was based on the design of Vlasak, et al.,[29] and Stoermer, et al.[30] which is shown schematically in Fig. 1. The active area of this device consists of closely spaced wires carrying high voltage of alternating polarity. When the gate is "open," the wires carry no voltage, and all ions pass through to the detector. When the gate is "closed," a pulse of ±500 V is applied to each wire, such that adjacent wires have opposite polarity. Ions entering the gate during this pulse are deflected away from the detector. The fast rise time (40 ns) of the pulse generator (Directed Energy, Inc., model PVM-4210) and estimated[29] cancellation of the electric field within 1 mm of the wires allow single mass unit resolution.
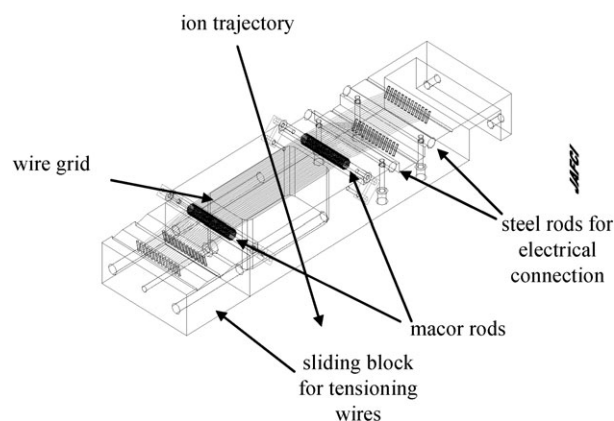

Fig. 1 Schematic drawing of the mass gate pulser. The interleaved grid of wires is stretched across the center of the assembly. The wires are kept coplanar by two macor rods. The electrical connections to the wires are made through stainless steel rods on which sit each set of wires. The sliding block at the bottom can be pulled out to tension the wires appropriately.

Vinylacetylene was synthesized utilizing a slightly modified literature procedure.[31] 1,4-dichlorobutene (30 mL) was added dropwise to a mixture of ethylene glycol (125 mL), butoxy-ethanol (25 mL), and potassium hydroxide (100 g) at 170 °C under a nitrogen atmosphere. Vinylacetylene was trapped in a condenser cooled in a dry ice/acetone bath, and was subse-quently stored in a gas cylinder as a 7% mixture in helium.

III. Computational methods

Paper I[23] describes the C_4H_4 singlet ground state (S_0) PES employing a manifold of methods including DFT,[32] CCSD(T),[33] and G2M[34] (see Paper I[23] for details). The calculated stationary points of the C_4H_4 PES were used as the input to Barker's MultiWell program suite[35,36] to model the photodissociation of vinylacetylene. All reactions under 100 kcal mol^{-1} were included in the simulations, as were all the dissociations of vinylacetylene itself under 120 kcal mol^{-1}. The full set of reactions, including transition state energies for each of the three levels of theory, can be found in the ESI†.

Utilizing the quantum chemical results of Paper I,[23] sums and densities of states for minima and tight transition states were calculated within the suite using the DenSum utility. In order to find loose transition states, the sums of states were calculated at several partially optimized geometries along the dissociation coordinate, and the structure with the lowest sum of states at a particular energy was used as the TS at that energy, along with its density and sum of states.

In order to simulate experimental conditions, account must be taken of the fact that photodissociation occurs in the presence of collisions. Lennard-Jones parameters were esti-mated for C_4H_4 from similar sized alkanes with $\sigma = 5$ Å and $\varepsilon = 280$ K used for all wells. The collisional parameters for helium were obtained directly from Barker,[36] $\sigma = 2.55$ Å and $\varepsilon = 10$ K. Simulations of Titan's nitrogen atmosphere and a shock tube study in argon used Lennard-Jones parameters $\sigma = 3.74$ Å and $\varepsilon = 82$ K and $\sigma = 3.47$ Å and $\varepsilon = 114$ K,

respectively.[36] Collisional energy transfer was modeled considering a single exponential model, where the probability of transferring energy $(E'-E)$ in a single collision is given by

$$P(E', E) = e^{-(E-E')/\langle \Delta E \rangle}$$

The average energy lost per collision, $\langle \Delta E \rangle$, was estimated, from the literature value for cyclobutane in helium, to be 200 cm^{-1}.[37] Ten thousand trials were used for photolysis simulations. Only 500 trials were used for simulation of a shock tube study due to the considerably longer computation time required.

Additional DFT calculations were carried out in this work to model the formation of phenylacetylene from C_4H_3 and C_4H_4. For this purpose, the B3LYP hybrid exchange–correlation functional[38–40] was used in combination with the 6-31 + G(d) basis set.[41]

IV. Experimental results

Fig. 2 shows difference mass spectra obtained from the 220 nm photoexcitation of vinylacetylene. The negative-going peaks in the spectra are due to incomplete subtraction of ion signals due to small amounts of impurities from the synthesis of vinylacetylene and other trace species present in the gas mixture. They appear as small negative signals because the excitation laser slightly changes the transport of the gas mixture into the ion source region when the reaction mixture absorbs ultraviolet radiation.[13] The majority of the parent vinylacetylene at mass 52 has been pulsed away by the ion gate

Fig. 2 Difference mass spectra of the photoproducts of the 220 nm photolysis of vinylacetylene. (a) Primary photoproducts C_4H_3 and C_4H_2. (b) Secondary products, C_8H_6 and C_6H_4, formed by reaction of the primary products. The negative-going peaks in the mass spectra are due to impurities in the gas mixture which are detected less efficiently in the presence of the photoexcitation laser. The parent C_4H_4 was pulsed away from the detector by the ion gate.

in order to increase the sensitivity of detection of nearby small photoproduct signals.

The only two primary photoproducts observed in Fig. 2(a) are the C_4H_3 radical and C_4H_2, which together are less than 1% the size of the original C_4H_4 signal. C_4H_3 and C_4H_2 appear in the mass spectrum with a ratio of 3 : 1. The true relative population ratio of these species is dependent on their photoionization cross sections at 10.5 eV, which for diacetylene is 24 Mb.[42] The cross section of C_4H_3 is not known, but the ionization cross sections of vinyl and propargyl radicals have been measured to be 13 and 8 Mb, respectively, at 10.5 eV.[43] If the cross section for C_4H_3 is similar, then the actual ratio of $C_4H_3 : C_4H_2$ is likely to be even greater, perhaps as high as 10 : 1.

We estimate that, during the traversal of the reaction tube, the radicals created during photolysis undergo a few hundred collisions with the buffer gas and tens of collisions with the parent C_4H_4, but do not encounter other photoproducts on the 15 μs timescale of the reaction. Reactive collisions between the radicals and the parent molecule result in formation of secondary products. By adjusting the timing between the photoexcitation and photoionization lasers, we can probe molecules that have been excited earlier in the reaction tube and have had the length of the tube to undergo further reaction.[11,13] The products of these secondary reactions are shown in Fig. 2(b). The major products are C_8H_6 and C_6H_4 in a 3 : 1 ion signal ratio. The signals due to these products are about a factor of ten smaller than the primary products shown in Fig. 2(a), consistent with the early time conditions probed by the reaction tube and the relatively small number of collisions involving radicals. The relative yields depend again on the photoionization cross sections. It will be shown shortly that at least some fraction of the C_8H_6 is phenylacetylene, but the C_6H_4 species could not be identified. Possible candidates for C_6H_4 are ene-diyne isomers or benzyne diradicals. Without knowing its identity, its ionization cross section and therefore product yield cannot be estimated.

Fig. 3 shows the ion signals due to C_4H_3 and C_8H_6 as a function of the time between the photoexcitation and photoionization lasers. Two conclusions can be drawn from the timing scan. First, both products are produced only during the narrow time interval during which reactants travel through the reaction tube. Second, the different time dependencies of the two products reflect the different nature of their formation. C_4H_3 results from the direct dissociation of C_4H_4 whereas C_8H_6 is generated by subsequent reactions of the dissociation products.

Identification of the C_8H_6 product was accomplished by recording its resonant two-photon ionization spectrum, shown in Fig. 4. The C_8H_6 product can be unambiguously identified as phenylacetylene by comparison with its known S_0–S_1 spectrum.[44] The sharp transitions in Fig. 4 show that the photoproduct has undergone significant cooling after exiting the reaction channel in the post-channel expansion. The origin (0_0^0) transition near 35 887 cm^{-1} is approximately 6 cm^{-1} full width at half maximum. Simulation[45,46] of the rotational band contour using previously determined rotational constants and transition moment direction[47] suggests that this bandwidth corresponds to a rotational temperature of approximately 25 K for the photoproducts following the final cooling stage that
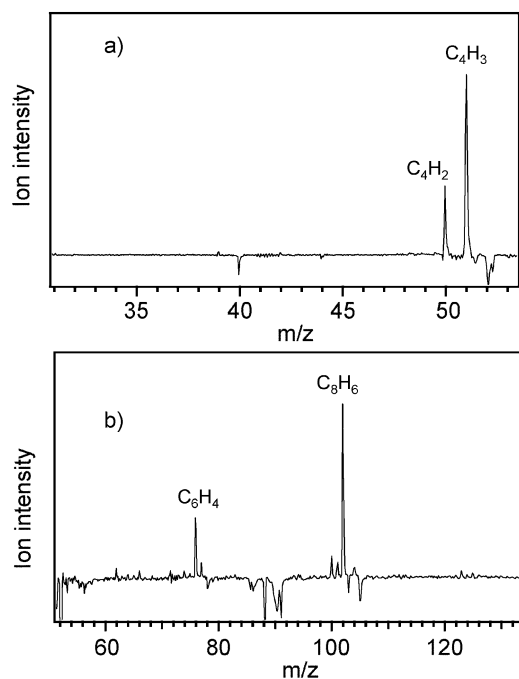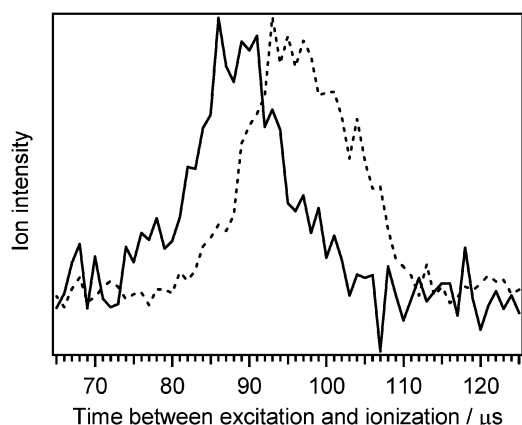
Fig. 3 Photoproduct ion signal as a function of time delay between the photoexcitation and photoionization laser pulses. —: C_4H_3. ···: C_8H_6. The two products are produced with different time dependencies, demonstrating that C_4H_3 is a primary dissociation product whereas C_8H_6 is formed by reaction of the primary products.

accompanies post-tube expansion as the photoproducts enter the ion source region.

V.   Simulations

A.   Conditions inside the reaction tube

As mentioned in the introduction, one important objective for the photochemistry experiment carried out in this work is the simulation of the photochemistry of vinylacetylene under conditions similar to those in Titan's atmosphere. At an altitude of 100 km, Titan's atmosphere is at a temperature of 150 K and a pressure of 10 mbar,[24] which corresponds to a number density of approximately 5×10^{17} molecules cm^{-3}. This gas density is about a factor of 8 less than the estimated gas density inside the reaction tube, 7×10^{16} molecules cm^{-3}.

The temperature inside the reaction tube was characterized by recording an action spectrum of the photodissociation of phenol to give phenoxy radicals, with photolysis timed to occur while the reaction mixture is inside the reaction tube.
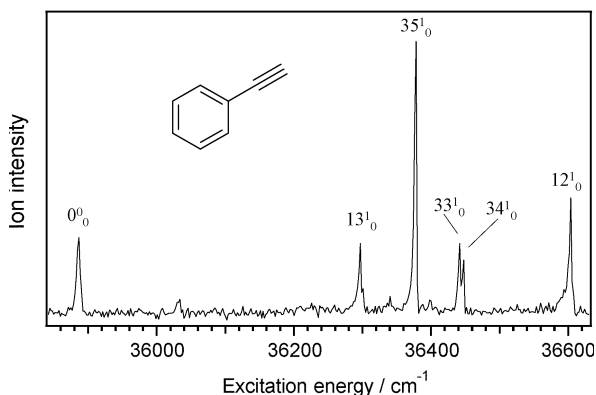

Fig. 4 Resonant two-photon ionization spectrum of the C_8H_6 photoproduct with major transitions labeled. The spectrum was identified as that of phenylacetylene by comparison with the known S_0–S_1 UV spectrum of phenylacetylene (see ref. 44).

By monitoring the phenoxy radical VUV ion signal as a function of excitation wavelength while tuning over the phenol origin transition, the rotational temperature of phenol in the reaction tube could be determined. Fig. 5(a) shows the experimental spectrum recorded in this manner, whereas Fig. 5(b), (c) and (d) show spectra simulated[45,46] at 50 K, 75 K, and 100 K, respectively, using previously determined rotational constants.[48] The experimental spectrum is best simulated by a 75 K $\pm$ 25 K rotational temperature. This temperature is somewhat colder than the estimated 150 K temperature of Titan's atmosphere at an altitude of 100 km. The simulations described below will shed light on the effects of these differences in temperature and pressure.

B.   Simulation results

Only two primary photoproducts of vinylacetylene were found in the present experiment: C_4H_3 and C_4H_2. In order to ascertain the importance of C_2H_2, to better understand the reaction mechanisms, and to compare the photolysis experiment to a shock tube study, the unimolecular decomposition of vinylacetylene was simulated by stochastically solving the time-dependent master equation[35,36] with C_4H_4 PES information taken from the quantum chemical calculations of Paper I.[23] Fig. 6 summarizes the reactions determined by the simulations to be most important to the photochemistry, showing the zero-point corrected DFT energies relative to vinylacetylene for each transition state. The numbering of the local minima on the C_4H_4 ground state singlet PES follows the convention described in Paper I and is repeated in Fig. 6. Dissociation products are denoted by the prefix **DP** and are also numbered. Transition states are designated **TS(x, y)** where x and y are the
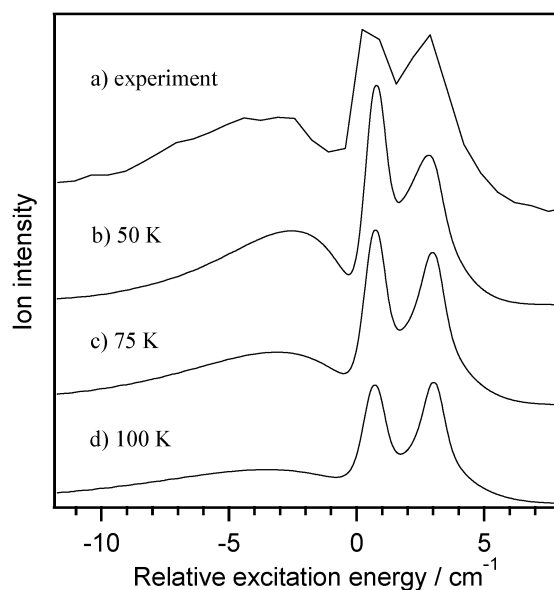

Fig. 5 Determination of the temperature inside the reaction tube. The production of phenoxy radicals was monitored as the photoexcitation laser was tuned over the origin transition of phenol. The experimental action spectrum is shown in (a), whereas simulated spectra at 50 K, 75 K, and 100 K are shown in (b)–(d), respectively. The experiment is best simulated by a 75 K temperature.
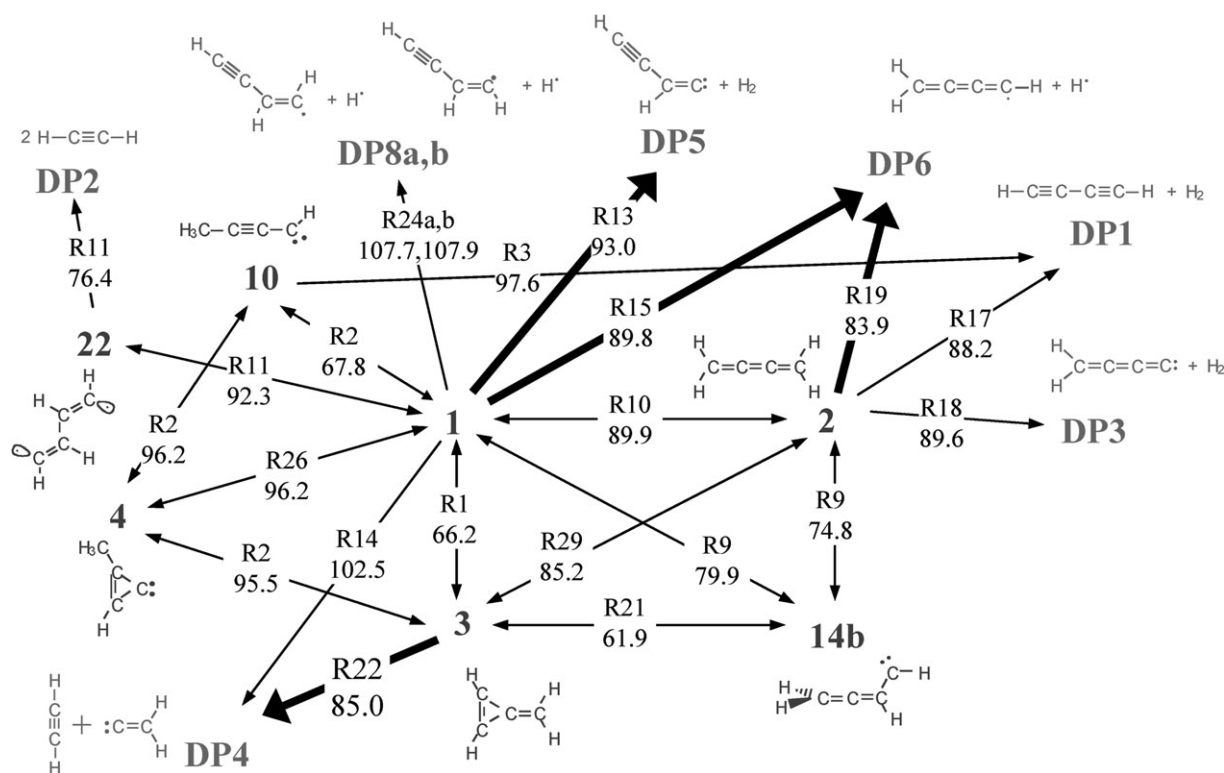
Fig. 6 The most important reactions in the photochemistry of vinylacetylene, as determined by the simulations. For each reaction, the zero-point corrected transition state energy at the DFT level of theory relative to that of vinylacetylene (**1**) is given in kcal mol^{-1}. The arrows in bold represent the most important dissociation pathways determined from the simulations. See the ESI† and Paper I[23] for a full description of the PES.

numerical labels of the reactant and product. The complete list of reactions can be found in the ESI†. For a full discussion of the reaction schemes, see Section 4 of Paper I.

To mimic the experimental reaction tube conditions, a temperature of 75 K and total gas density of 7×10^{16} molecules cm^{-3} of helium were used. Ultraviolet excitation followed by rapid internal conversion to the ground state was simulated by assuming a 75 K thermal distribution onto which 130 kcal mol^{-1} (220 nm) was added.

The most direct comparison to the experiment is the final product distribution of C_nH_m species in a simulation of the experiments described in Section IV. These results are summarized in Table 1 for simulations using each level of theory employed. The differences in the product ratios can be traced to the energies of **DP6** at the various levels of theory: 100.4 kcal mol^{-1} (CCSD(T)), 105.6 kcal mol^{-1} (G2M), and 92.4 kcal mol^{-1} (DFT). The best match to the experimental C_4H_2 : C_4H_3 ratio is found using DFT. This is most likely due to a fortuitous cancellation of errors, because CCSD(T) represents

the most accurate method used. It may also indicate the involvement of excited states. These questions cannot be resolved at this stage, so the DFT results will be used in the following discussion.

The time-dependent branching ratios of the major pathways involved in the photodissociation of vinylacetylene as calculated using DFT energies are shown in Fig. 7(a). The pathways to form **DP6** and **DP1** are shown separately to better clarify the reactions taking place. Note that the ordinate in Fig. 7 reports the fraction of the photoexcited molecules that follow a particular pathway rather than the fractional abundance of a particular species. This is necessary because, in a reaction such as **R22**, C_4H_4 decomposes into two C_2H_2 molecules (**DP4**).

The primary photochemistry is complete within ten nanoseconds, and virtually no C_4H_4 survives the excitation intact. Rearrangement of vinylacetylene (**1**) to methylenecyclopropene (**3**) and subsequent dissociation to acetylene plus vinylidene (**DP4**) is the major product pathway, as nearly half of photoexcited **1** follows this route. Dissociation of the weakest C–H bond (the secondary vinyl CH) in vinylacetylene to give the C_4H_3 radical **DP6** is the second most favored product channel, yielding 26% of the products. This radical product can also be formed by C–H dissociation of **2** (butatriene), which is formed in the first few nanoseconds from **1** but which never accumulates to more than a few percent because of subsequent reaction (Fig. 7(b)). Dissociation of **2** to **DP6** accounts for another 13% of photoexcited **1**. The remaining product channel shown in Fig. 7(a), responsible for 7% of the

Table 1 Product distributions of the simulations of the photochemistry of vinylacetylene

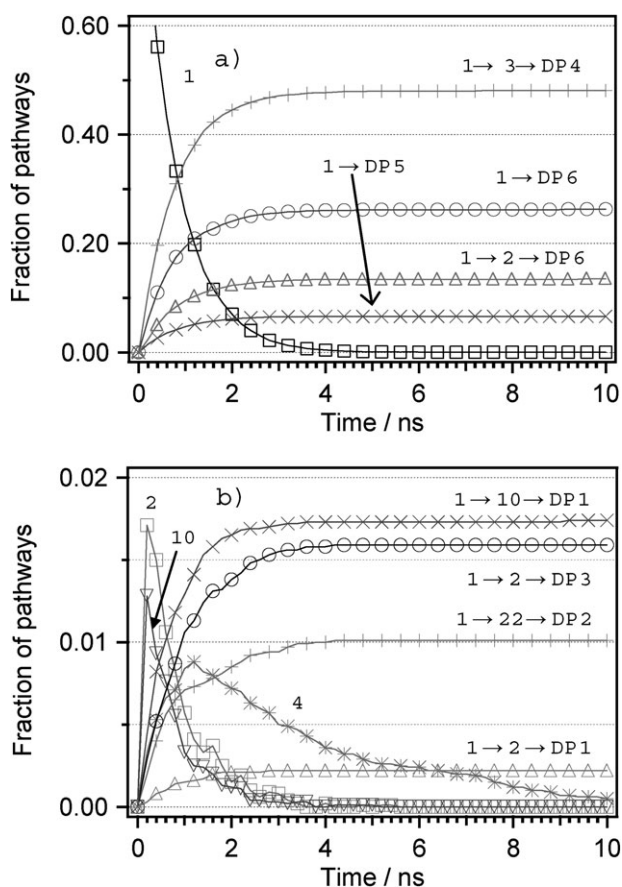|	C_2H_2	C_4H_2	C_4H_3
DFT	66	7	27
CCSD(T)	90	4	6
G2M	92	4	4
Experiment	—	1	3–10

Fig. 7 Simulation of the 220 nm photochemistry of vinylacetylene at the temperature and pressure of the present experiment. The time dependent curves represent the branching ratios of the different pathways, but do not necessarily reflect the actual concentration of a particular product because several pathways lead to two C_2H_2 molecules (*e.g.*, **R22** yielding **DP4**). (a) The parent molecule **1** ($\square$) and major product channels: **DP4** ($+$), **DP6** directly from **1** ($\bigcirc$), **DP6** *via* **2** ($\triangle$), **DP5** ($\times$). (b) Intermediates **2** ($\square$), **4** (*) and **10** ($\triangledown$) and minor product channels: **DP1** *via* **10** ($\times$), **DP3** *via* **2** ($\bigcirc$), **DP2** *via* **22** ($+$), and **DP1** *via* **2** ($\triangle$).

products, is the direct loss of H_2 from **1** to give **DP5**. **DP5** is located on a flat part of the PES so that a 1,2-H shift and formation of diacetylene (**DP1**) occurs immediately (see Paper I[23]). The major pathways are the same when simulating excitation from the other two deep minima populated by **2** and **3**, however, the relative importance of each path changes with the choice of the starting structure. For 220 nm excitation of **2**, direct dissociation to **DP6** accounts for 57% of the excited molecules, whereas rearrangement to **1**, then **3**, and finally dissociation to **DP4** accounts for another 27%. As might be expected, dissociation to **DP4** dominates when the starting reactant is **3**, accounting for 74% of the excited molecules.

The time profiles of several other minor species formed following excitation of **1** are shown in Fig. 7(b). Although small amounts of **2**, **4** and **10** are present at early stages of the reaction, **3** never accumulates in significant quantities because of rapid dissociation to **DP4**. **DP1** is the most abundant of the minor products, and can be formed in several ways. One

pathway involves the carbene **10** as an intermediate followed by loss of H_2 from the methyl group of **10**. The pathway involving **2** to form **DP1** is only responsible for 0.2% of the product pathways, but dissociation from **2** to give the C_4H_2 isomer **DP3** represents 1.6%. This is interesting in light of the fact that **TS(2,DP3)** is actually slightly higher in energy than **TS(2,DP1)** as shown in Fig. 6. The sum of states at the energy of the photoexcitation is nearly an order of magnitude higher for **TS(2,DP3)** than it is for **TS(2,DP1)**, explaining why the former product channel is favored. As shown in Scheme 3 of Paper I,[23] the structure of **TS(2,DP1)** is quite compact and rigid, whereas that of **TS(2,DP3)** is elongated and flexible, giving rise to a flatter potential, lower vibrational frequencies and increased density and sum of states. The other product channel shown in Fig. 7(b), **DP2**, arises from dissociation of the biradical **22**. Other reactions shown in Fig. 6 also led to products, such as **DP8a** and **DP8b**, but these were each responsible for less than 0.5% of the final product distribution.

Many interesting molecules such as **DP3** and **DP5** are formed as the products, however, the barriers to isomerization to more stable species (*e.g.*, **DP5** $\rightarrow$ **DP1**) are low or non-existent.[23] Previous calculations predict the barrier for the 1,2-hydrogen shift needed to isomerize from vinylidene to acetylene (*i.e.*, **DP4** $\rightarrow$ **DP2**) to be just 2 kcal mol^{-1}.[49] Isomerization among the stable isomers of C_4H_3 has been calculated to require about 40 kcal mol^{-1} [27] for a total energy of 130–140 kcal mol^{-1} above vinylacetylene, and is probably not feasible in our experiment.

The final product ratios for several calculations, as would be seen in a mass spectrometry experiment, are given in Fig. 8, including simulations of the present experiment and of photochemistry at the temperature and pressure of Titan's nitrogen atmosphere at 100 km. The fractional abundances sum the contributions from all pathways to a particular species, and also account for the fact that **DP2** and **DP4** form two acetylene molecules. The ratio of C_4H_3 : C_4H_2 in the simulation of the reaction tube is 4 : 1, in accordance with the experimental ratio of about 3–10 : 1. The amount of C_2H_2 in both photochemistry simulations is about 2.4 times the amount of C_4H_3. The product distribution does not differ significantly between the reaction tube and Titan's atmosphere, with the ratio C_2H_2 : C_4H_3 : C_4H_2 equal to 66 : 27 : 7 for both.

Fig. 8 also shows the results of a 50 ms simulation of a shock tube study of **1**. The shock tube (translational) temperature was 1500 K, with a vibrational (preshock) temperature of 300 K, at a pressure of 1.5 bar. These conditions were designed to simulate the work of Hidaka *et al.*[21] in order to establish the suitability of the C_4H_4 reaction scheme (Fig. 6) for simulating a thermal dissociation of vinylacetylene, and to assess the differences in product yields between the shock tube studies and photochemistry in a planetary atmosphere.

One parameter measured directly by Hidaka *et al.*[21] was the rate constant for the loss of C_4H_4, which at 1500 K was 134 s^{-1}. The loss of C_4H_4 in the simulation was fit to give a value of 43 s^{-1}, nearly a factor of three lower than the experimental value. The initial reaction rates inferred from the shock tube studies[21] given in eqn (1) can be compared to those obtained in the simulation. The rates for formation of
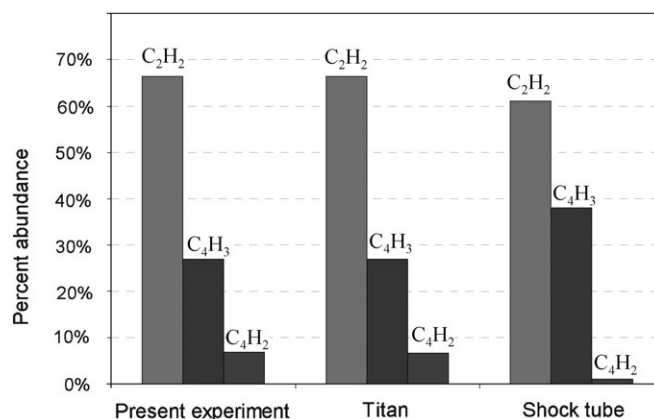
Fig. 8 Final product distributions of three simulations of the dissociation of vinylacetylene, showing the relative abundances of C_2H_2, C_4H_3, and C_4H_2. Left: simulation of the present experiment, 220 nm photolysis at 75 K and 7×10^{16} molecules cm^{-3} in helium. Center: simulation of photochemistry at the temperature and pressure of Titan's nitrogen atmosphere at 100 km altitude, 220 nm photolysis at 150 K and a total number density 5×10^{17} molecules cm^{-3} N$_2$. Right: simulation of a thermal shock tube pyrolysis at 1500 K and 7×10^{18} molecules cm^{-3} of argon.

C_4H_3, $2C_2H_2$ and C_4H_2 from the simulation are 16.7 s^{-1}, 26.5 s^{-1}, and 0.3 s^{-1}, respectively, which vary considerably from the experimental rates given in eqn (1). The rates from the simulation correspond to a ratio of products of C_2H_2 : C_4H_3 : C_4H_2 = 55 : 35 : 1, with 9% C_4H_4 unreacted after 50 ms, projecting to a ratio of C_2H_2 : C_4H_3 : C_4H_2 = 61 : 38 : 1 after the reaction of all the vinylacetylene, as shown in Fig. 8. The simulation does not predict that C_2H_2 dominates so thoroughly as in the shock tube experiment, and also predicts significantly less C_4H_2 relative to C_4H_3 than would be expected from the reaction rates found in the shock tube study. Possible reasons for this will be discussed below.

VI. Discussion

A. Primary products of photolysis and thermal dissociation of vinylacetylene

The present experiments on ultraviolet photolysis of vinylacetylene show both radical (C_4H_3) and molecular (C_4H_2) species as primary products, with C_4H_3 appearing three times as large as C_4H_2. Simulations of the experiment that assume dissociation follows internal conversion predict that acetylene arising from **DP2** and **DP4** accounts for 66% of the hydrocarbon photoproducts. However, C_2H_2 cannot be detected using 118 nm VUV photoionization because its ionization potential is larger than the VUV photon energy. The simulation suggests that dissociation occurs directly from the vinylacetylene well on the C_4H_4 PES, as well as after isomerization to several other C_4H_4 isomers, sampling both closed-shell and biradical pathways. The initial dissociation products are frequently intermediates that quickly isomerize to the more stable acetylene and diacetylene. The C_4H_3 radicals are also formed in significant numbers, and, as free radicals, are quite important to any subsequent photochemistry. In these simulations, we assume the dissociation occurs strictly on the ground state singlet PES, an assumption that is supported by comparison to butadiene, but for which there is no direct experimental or

computational evidence. The possibility of important excited state reactions cannot be ruled out.

The simulations also validate comparison of our experiment to the atmosphere of Saturn's moon Titan. The temperatures and pressures are sufficiently similar that the photochemical product distributions are also very similar. The overall expected product yield of ultraviolet photochemistry of vinylacetylene on Titan was assessed by examining the wavelength dependence of the solar flux, absorption cross section and product distribution. The solar flux increases over the range 190–240 nm,[12] while the absorption cross section of vinylacetylene in this range can be estimated from a previous study[16] at higher temperature, and from our own R2PI studies. The onset of the absorption is around 225 nm and reaches a maximum around 215 nm. The combination of these estimates suggest that significant absorption of sunlight by vinylacetylene on Titan only occurs between 200–225 nm. The product yields were simulated in this wavelength range and found to vary only slightly with wavelength. The overall product yield, including all of these factors, for solar photolysis of vinylacetylene on Titan was found to be C_2H_2 : C_4H_2 : C_4H_3 = 65 : 8 : 27.

Previous results from shock tube studies[21] are considerably different, where the reaction rates for the initial steps given in eqn (1) predict an initial branching ratio at 1500 K of 92% acetylene, 5% diacetylene, and 3% C_4H_3 radicals. As has been stated previously,[6] these differences highlight the risks associated with using high temperature, thermally-driven reactions in modeling photochemical pathways in Titan and the outer planets' atmospheres. The simulation of the shock tube experiment at 1500 K and 1.5 atm predicted acetylene to be the major product, similarly to the photochemistry, but the amount of C_4H_2 formed was drastically decreased relative to the two photochemical simulations. The chemistry in the shock tube occurs at much lower average vibrational energies than the ultraviolet photochemistry. The vibrational energy of **1** in the shock tube study will be in a Boltzmann distribution for 1500 K, which results in an average vibrational energy of about 10 000 cm^{-1}. The major C_4H_2 product channel is over a

barrier of 93 kcal mol^{-1}, or about 32 550 cm^{-1}, so only a small fraction of the reactant molecules in the high energy Boltzmann tail will have sufficient energy to overcome this barrier. By contrast, the ultraviolet photon in the photochemistry experiment provides over 45 000 cm^{-1} (130 kcal mol^{-1}) to each vinylacetylene molecule that is excited, so the C_4H_2 reaction channel is always accessible.

The simulations predict significantly different reaction rates for the individual reactions given in eqn (1) than those found for the shock tube experiment.[21] Despite the fact that dissociation to give $2C_2H_2$ dominates in both the experiment and the simulation, the simulated rate of this reaction is much less than its value inferred from the shock tube results, while the experimental rate of formation of C_4H_2 is 67 times its simulated value. It is conceivable that there is a lower-energy dissociation pathway to form C_4H_2, perhaps involving low-energy singlet or triplet excited states of the important carbene intermediates **14** or **10**, which both have a triplet ground state (Paper I[23]). Such a pathway might be more energetically accessible in a thermal dissociation. It would also consequently increase the yield of C_4H_2 in the simulation of the photochemical experiment, but such an increase would not necessarily be inconsistent with our experimental determination of the ratio of $C_4H_3 : C_4H_2$ of 3–10 : 1. The substantial differences in the other reaction rates may reflect overestimation of the energetics of the formation of C_2H_2 and underestimation of the energy of H atom loss to give C_4H_3. An analysis of the simulation results suggests that adjusting these barriers by less than 5 kcal mol^{-1} (5–7%) may be enough to bring the product yields into agreement with previously observed reaction rates. Interestingly, the increased H-atom dissociation energy predicted in Paper I[23] by the CCSD(T) and G2M methods results in a dominance ($> 90\%$) of C_2H_2 in simulations of the shock tube experiment using these energies. However, essentially none of the product is predicted to be C_4H_2, as with the DFT-based simulations. If the C_4H_3 product pathways are better characterized by the CCSD(T) or G2M energies, then the presence of significant amounts of C_4H_3 in the photochemistry experiment may be indicative of excited state reaction.

The end product ratio $C_2H_2 : C_4H_2 = 7$–10 : 1 observed by Hidaka *et al.*[21] suggests the production of much more C_4H_2 than the simulation predicts. However, this is likely due to further reactions of C_4H_3 that occur in the shock tube but not in the constrained expansion, giving rise to more C_4H_2. The simple loss of a hydrogen atom from C_4H_3 to give C_4H_2 requires an additional 50 kcal mol^{-1} at the B3LYP/6-311 + +G(3df,3pd) level of theory. This calculation is in accord with previous results that put the energy difference around 40 kcal mol^{-1}.[50] In the shock tube at 1500 K, the hot C_4H_3 radical undergoes further dissociation to diacetylene. In the reaction tube photochemistry, however, the radicals will undergo deactivating collisions with the buffer gas and subsequent dissociation will not occur.

Another explanation is that reactive collisions of C_4H_3 play an important role in the shock tube experiment, whereas they are not considered in the simulations and are less important in the lower-pressure environment of the reaction tube in our photochemistry experiment. In the shock tube, the combination of higher gas density, longer reaction time and higher molecular velocities increase the possibilities for reactive collisions between dissociation products, such as H atom plus C_4H_3 to give $C_4H_2 + H_2$. This reaction is relatively unlikely in the present photochemistry experiment because of the low number density of radicals created in the reaction tube.

B. Secondary reactions of C_4H_3

In addition to an assessment of the primary photolysis of vinylacetylene, this experiment also sought to study the molecules formed from subsequent reaction of the primary products. The aromatic molecule phenylacetylene was spectroscopically identified as a secondary product of vinylacetylene photolysis. Of the observed and predicted primary products, C_4H_3 is the only hydrocarbon free radical formed, and thus is anticipated to be the species responsible for subsequent reactions forming larger C_nH_m products. Because the C_4H_3 free radical was only present at about 0.5% the concentration of the parent C_4H_4 molecule, radical–radical recombination reactions are not anticipated to be significant. Instead, the C_6H_4 and C_8H_6 secondary products must arise from the reaction of C_4H_3 with vinylacetylene:

$$C_4H_3 + C_4H_4 \rightarrow C_8H_6 + H$$

$$\rightarrow C_6H_4 + C_2H_3$$
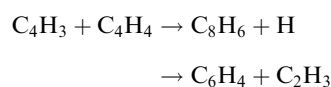
It has been previously suggested that C_4H_3 can react with C_2H_2 to form a phenyl radical with an entrance barrier of 14 kcal mol^{-1} and all subsequent steps downhill.[51] The mechanism for the formation of phenylacetylene in the present experiment may be similar, with the initial reaction step being the formation of the bond between the radical center in C_4H_3 and one of the acetylenic carbon atoms in vinylacetylene (Fig. 9(a)). Alternatively, the initial attack could occur at the vinyl group of the C_4H_4 molecule (Fig. 9(b)). Following the mechanism proposed by Walch[51] for $C_2H_2 + C_4H_3$, a five-membered ring is formed initially, followed by hydrogen transfer, reopening of the ring, and finally closure of the six-membered ring. Hydrogen transfer(s) and loss of a hydrogen atom are the final steps to form phenylacetylene. Calculations at the B3LYP/6-31 + G(d) level of theory indicate that either initial step is plausible, and in fact both have a lower barrier than the reaction between C_4H_3 and C_2H_2. The barrier for the first step of attack at the acetylenic group was found to be 6.5 kcal mol^{-1} relative to $C_4H_4 + C_4H_3$, while for vinyl attack the first step had a barrier of 5.7 kcal mol^{-1}. By comparison, the acetylenic attack occurring in the previously proposed $C_4H_3 + C_2H_2$ reaction has a barrier of 11.1 kcal mol^{-1} at the B3LYP/6-31 + G(d) level.

In the reaction tube photochemistry at 220 nm, the C_4H_3 radical will be created with approximately 32 kcal mol^{-1} excess energy, and will undergo tens of collisions with the buffer gas before encountering a C_4H_4 molecule. According to the collisional deactivation model used in the simulations, the C_4H_3 radical would have on average 25 kcal mol^{-1} internal energy at the first encounter with C_4H_4, and 11 kcal mol^{-1} at the second. The calculated barriers for the first step of the reactions in Fig. 9(a) and (b) would be easily surpassed.
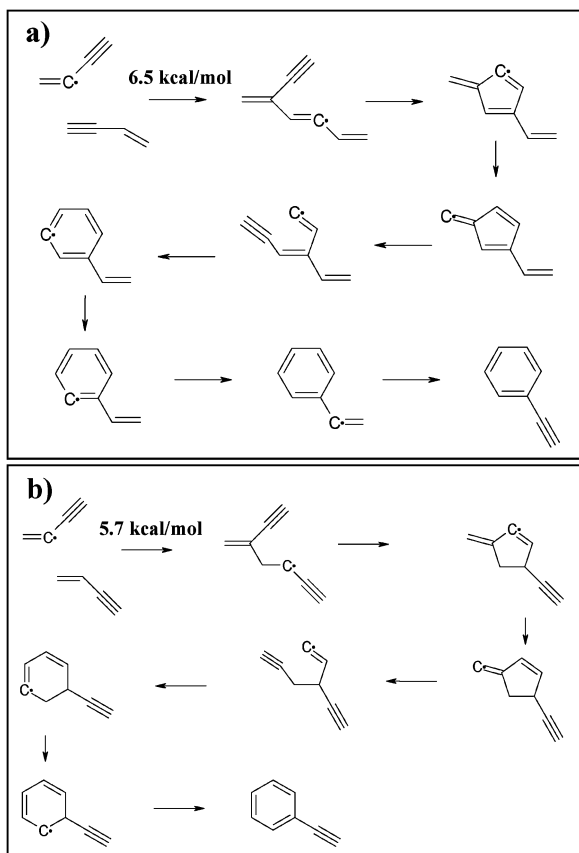
Fig. 9 Proposed mechanisms for the reaction between C_4H_3 and C_4H_4 to form phenylacetylene, with the initial step at (a) the acetylenic group, or (b) the vinyl group.

A full exploration of the C_8H_7 and C_8H_6 potential energy surfaces is beyond the scope of this work but would be a much-needed addition to current understanding of hydrocarbon chemistry. The smaller product C_6H_4 may be formed analogously with loss of a vinyl radical. The radical–molecule reaction between C_4H_3 and C_4H_4 provides a novel route to aromatic ring closure that has not been anticipated previously. Radical–radical reactions are often assumed to play the major role in aromatic ring formation[4,6] but, as shown here, even relatively inefficient radical–molecule reactions can be quite important when the number density of radicals is low, and should be considered in models of Titan's atmosphere.

VII.   Conclusions

The simulation of ultraviolet photochemistry of vinylacetylene under conditions similar to those of Titan's atmosphere predicts production of acetylene, diacetylene, and C_4H_3 in a ratio of 66 : 7 : 27, consistent with an experimental ratio of C_4H_2 : C_4H_3 of 1 : 3–10. The recommended branching ratio for photochemistry of vinylacetylene on Titan, taking into effects of solar flux, absorption cross sections, and product yields, is 65% acetylene, 8% diacetylene, and 27% C_4H_3 radicals. This product ratio is considerably different than that of thermal dissociation of vinylacetylene, where acetylene is thought to

dominate to an even greater degree.[21] Simulations of the initial steps of the shock tube experiment give a much higher initial yield of C_4H_3 and a reduced yield of C_4H_2 relative to what was observed, but the reasons for this are unclear. These differences highlight the care that must be taken in selecting branching ratios for modeling planetary atmospheres. Photochemistry of vinylacetylene was also shown experimentally to produce phenylacetylene, from reaction between the parent vinylacetylene and the dissociation product C_4H_3. This reaction provides a novel photochemical route to aromatic ring formation from small hydrocarbons, which may be important in understanding Titan's atmosphere.

Acknowledgements

References

1 Y. L. Yung, M. Allen and J. P. Pinto, *Astrophys. J., Supp. Ser.*, 1984, **55**, 465.
2 D. Toublanc, J. P. Parisot, J. Brillet, D. Gautier, F. Raulin and C. P. McKay, *Icarus*, 1995, **113**, 2–26.
3 L. M. Lara, E. Lellouch, J. J. Lopez-Moreno and R. Rodrigo, *J. Geophys. Res.*, 1996, **101**, 23261–23283.
4 E. H. Wilson and S. K. Atreya, *J. Geophys. Res.*, 2004, **109**, E06002.
5 A. Coustenis, A. Salama, B. Schulz, S. Ott, E. Lellouch, T. Encrenaz, D. Gautier and H. Feuchtgraber, *Icarus*, 2003, **161**, 383–403.
6 E. H. Wilson, A. Coustenis and S. K. Atreya, *J. Geophys. Res.*, 2003, **108**, 1896.
7 L. D. Jaffe and L. M. Herrell, *J. Spacecr. Rockets*, 1997, **34**, 509–521.
8 H. B. Niemann, S. K. Atreya, S. J. Bauer, G. R. Carignan, J. E. Demick, R. L. Frost, D. Gautier, J. A. Haberman, D. N. Harpold, D. M. Hunten, G. Israel, J. I. Lunine, W. T. Kasprzak, T. C. Owen, M. Paulkovich, F. Raulin, E. Raaen and S. H. Way, *Nature*, 2005, **438**, 779–784.
9 J. H. Waite, Jr, H. Niemann, R. V. Yelle, W. T. Kasprzak, T. E. Cravens, J. G. Luhmann, R. L. McNutt, W.-H. Ip, D. Gell, V. D. L. Haye, I. Muller-Wordag, B. Magee, N. Borggren, S. Ledvina, G. Fletcher, E. Walter, R. Miller, S. Scherer, R. Thorpe, J. Xu, B. Block and K. Arnett, *Science*, 2005, **308**, 982.
10 R. E. Bandy, C. Lakshminarayan, R. K. Frost and T. S. Zwier, *Science*, 1992, **258**, 1630–1633.
11 R. E. Bandy, C. Lakshminarayan, R. K. Frost and T. S. Zwier, *J. Chem. Phys.*, 1993, **98**, 5362–5374.
12 T. S. Zwier and M. Allen, *Icarus*, 1996, **123**, 578–583.
13 C. A. Arrington, C. Ramos, A. D. Robinson and T. S. Zwier, *J. Phys. Chem. A*, 1998, **102**, 3315–3322.
14 J. C. Robinson, S. A. Harris, W. Sun, N. E. Sveum and D. M. Neumark, *J. Am. Chem. Soc.*, 2002, **124**, 10211–10224.
15 J. Newby, J. A. Stearns and T. S. Zwier, (in preparation).
16 A. Fahr and A. Nayak, *Chem. Phys.*, 1996, **203**, 351–358.
17 S. Glicker and H. Okabe, *J. Phys. Chem.*, 1987, **91**, 437.
18 R. E. Bandy, C. Lakshminarayan and T. S. Zwier, *J. Phys. Chem.*, 1992, **96**, 5337–5343.
19 O. L. Chapman, *Pure Appl. Chem.*, 1974, **40**, 511.
20 R. Wrobel, W. Sander, D. Cremer and E. Kraka, *J. Phys. Chem. A*, 2000, **104**, 3819–3825.

21 Y. Hidaka, H. Masaoka, H. Oshita, T. Nakamura, K. Tanaka and H. Kawano, *Int. J. Chem. Kinet.*, 1992, **24**, 871–885.

22 *NIST Chemistry WebBook, NIST Standard Reference Database Number 69* ed. P. J. Linstrom and W. G. Mallards, (http://webbook.nist.gov), National Institute of Standards and Technology, Gaithersburg, MD, 20899, 2005.

23 D. Cremer, E. Kraka, H. Joo, J. A. Stearns and T. S. Zwier, *Phys. Chem. Chem. Phys.*, DOI: 10.1039/b609284e.

24 A. Coustenis and B. Bézard, *Icarus*, 1995, **115**, 126.

25 P. R. Westmoreland, A. M. Dean, J. B. Howard and J. P. Longwell, *J. Phys. Chem.*, 1989, **92**, 8171–8180.

26 J. A. Miller and C. F. Melius, *Combust. Flame*, 1992, **91**, 21–39.

27 S. E. Wheeler, W. D. Allen and H. F. S. III, *J. Chem. Phys.*, 2004, **121**, 8800–8813.

28 R. Mahon, T. J. Mcllrath, V. P. Myerscough and D. W. Koopman, *IEEE J. Quantum Electron.*, 1979, **QE–15**, 444.

29 P. R. Vlasak, D. J. Beussman, M. R. Davenport and C. G. Enke, *Rev. Sci. Instrum.*, 1996, **67**, 68.

30 C. W. Stoermer, J. Friedrich, D. Schooss and M. M. Kappes, *Rev. Sci. Instrum.*, 1998, **69**, 1661.

31 E. Tørneng, C. J. Nielsen and P. Klaeboe, *Spectrochim. Acta, Part A*, 1980, **36A**, 975.

32 W. Kohn and L. Sham, *Phys. Rev.*, 1965, **140**, A1133.

33 K. Raghavachari, G. W. Trucks, J. A. Pople and M. Head-Gordon, *Chem. Phys. Lett.*, 1989, **157**, 479.

34 A. M. Mebel, K. Morokuma and M. C. Lin, *J. Chem. Phys.*, 1995, **103**, 7414–7421.

35 J. R. Barker, *Int. J. Chem. Kinet.*, 2001, **33**, 232.

36 J. R. Barker, N. F. Ortiz, J. M. Preses, L. L. Lohr, A. Maranzana and P. J. Stimac, *Multiwell-2.02 software*, http://aoss.engin.umich.edu/multiwell/, University of Michigan, Ann Arbor, MI, 2006.

37 I. Oref and D. C. Tardy, *Chem. Rev.*, 1990, **90**, 1407.

38 C. Lee, W. Yang and R. G. Parr, *Phys. Rev. B*, 1988, **37**, 785.

39 A. D. Becke, *Phys. Rev.*, 1988, **A38**, 3098.

40 A. D. Becke, *J. Chem. Phys.*, 1993, **98**, 5648.

41 P. C. Hariharan and J. A. Pople, *Theor. Chim. Acta*, 1973, **28**.

42 T. A. Cool, J. Wang, K. Nakajima, C. A. Taatjes and A. Mcllroy, *Int. J. Mass Spectrom.*, 2005, **247**, 18–27.

43 J. C. Robinson, N. E. Sveum and D. M. Neumark, *J. Chem. Phys.*, 2003, **119**, 5311.

44 D. E. Powers, J. B. Hopkins and R. E. Smalley, *J. Chem. Phys.*, 1981, **74**, 5971–5976.

45 W. A. Majewski, J. F. Pfanstiel, D. F. Plusquellic and D. W. Pratt, in *Laser Techniques in Chemistry*, ed. A. B. Myers and T. R. Rizzo, Wiley, New York, 1995, vol. XXIII, pp. 101–148.

46 D. F. Plusquellic, R. D. Suenram, B. Mate, J. O. Jensen and A. C. Samuels, *J. Chem. Phys.*, 2001, **115**, 3057.

47 J. W. Ribblett, D. R. Borst and D. W. Pratt, *J. Chem. Phys.*, 1999, **111**, 8454.

48 G. Berden, W. L. Meerts, M. Schmitt and K. Kleinermanns, *J. Chem. Phys.*, 1996, **104**, 972–982.

49 N.-y. Chang, M.-y. Shen and C.-h. Yu, *J. Chem. Phys.*, 1997, **106**, 3237.

50 S. J. Klippenstein and J. A. Miller, *J. Phys. Chem. A*, 2005, **109**, 4285.

51 S. P. Walch, *J. Chem. Phys.*, 1995, **103**, 8544–8547.

This journal is © the Owner Societies 2006

Phys. Chem. Chem. Phys., 2006, **8**, 5317–5327 | 5327